THE JOURNAL OF PHYSICAL CHEMISTRY C
A JOURNAL OF THE AMERICAN CHEMICAL SOCIETY

pubs.acs.org/JPCC

Article

Tunable Optical Constants of Aluminum Tungsten Bronzes in Electrochromic Tungsten Oxide Thin Films

Kunrun Song, Shichen Weng, Jumei Zhou, Ran Jiang, Hongtao Cao, and Hongliang Zhang*

Cite This: J. Phys. Chem. C 2023, 127, 18036−18042

Read Online

ACCESS | Metrics & More | Article Recommendations | Supporting Information

ABSTRACT: Aluminum tungsten bronze (Al_xWO_3) as the core layer for optical modulation is of great significance to electrochromic (EC) devices. Compared with other EC properties, there remains a vacancy in the study of optical constants of Al_xWO_3. Herein, the tunable optical constants of Al_xWO_3 layers under varying potentials are investigated via a spectroscopic ellipsometer. Our findings indicate that in terms of optical constants, the Al_xWO_3 layer exhibits greater modulation over a more extensive voltage range and has better modulation ability than H_xWO_3 and Li_xWO_3. With the generation of Al_xWO_3, the WO_3 thin films exhibit a 2.12% increase in thickness and a 0.26 eV decrease in the optical band from the bleached to the fully colored state. The large optical constant modulation capability of aluminum−tungsten bronze enables it to achieve comparable modulation capability to that in a lithium-ion system but at lower applied voltage conditions. Furthermore, the expanded modulation range further enhances its potential applications in electronic, optical, and other devices. These results are expected to offer great assistance in understanding the coloration principle and the design of novel EC devices.

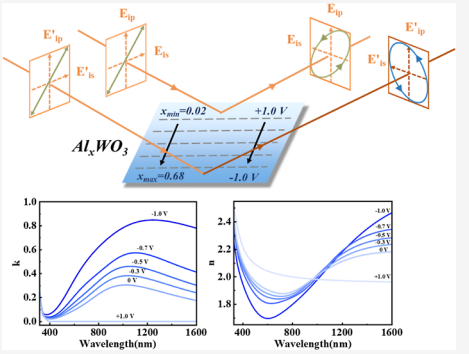

1. INTRODUCTION

Electrochromic (EC) thin films allow their colors or optical properties (absorbance/transmittance/reflectance) to be modulated via reversible redox reaction by a small applied voltage and have been widely applied as smart windows, antiglare rearview mirrors, and sunroofs of automobiles because of their low cost and low energy consumption.[1−3] In recent decades, tungsten oxide (WO_3) is the most widely explored EC inorganic material, which possesses the advantages of sizeable optical modulation, being non-toxic, high coloration efficiencies, and excellent cyclic reversibility.[4−6] Meanwhile, in the field of photoelectrochemical water splitting,[7−10] WO_3 has also emerged as a widely researched material. There is no doubt that the EC performance of WO_3 electrodes depends strongly on their structures and morphologies. Llordes et al. have proved that the nanocrystal-in-glass structural characteristic can improve the cyclic stability of EC thin films due to the buffering effect of nanocrystals in the amorphous matrix.[11] Compared to its pure amorphous/crystalline structure, the nanocrystal-in-glass structure of the electrodes exhibits the highest diffusion coefficient and charge/discharge density.[12] As for conventional EC devices, univalent proton (H^+) and ions (Li^+, Na^+) have been widely adopted as electrolyte systems. Nevertheless, the limitation of these elements still needs to be overcome. For instance, the presence of H^+ in the electrolyte causes corrosion of the metal oxide surface. Additionally, the larger radius of Na^+ hinders the EC response time of devices. Though Li^+ exhibits an appropriate ion radius and faster diffusion rate compared to Na^+ and H^+, the combination of limited Li^+ resources and the irreversible trapping of Li^+ within the device necessitates the constant search for suitable substitutes.[13] Recently, a novel Zn^{2+}/K^+ dual-ion Zn-Prussian blue EC device has been reported to be driven by the tiny potential difference of electrodes. It only takes ~6.8 mg/cm^2 of the Al sheet for 450 switching cycles.[14] Another instance refers to a dual-band EC smart window with an Al^{3+} electrolyte, which possesses a high coloration efficiency of 254 cm^2 C^{-1} at 1200 nm.[15] In our previous investigation, the Al^{3+} ion in the electrolyte takes effect on stabilizing the host framework and exhibits longer cycle life performance due to its strong electrostatic forces. While the multivalent Al^{3+} ion electrolyte and its complementary strategies are very promising in electrochromism,[15,16] efforts are gradually shifting to the development of multivalent ion electrolytes or hybrids that exhibit these advantages of a small ion radius (0.53 Å), trivalent electron configuration, environmental friendliness, and high safety. The smaller ion radius of Al^{3+} (0.53 Å) than Li^+ (0.59 Å), leading to less damage to ion channels during ion transport and the trivalence of aluminum ions, caused more charges to be transferred during the inserted process, providing

Received: May 24, 2023
Revised: August 23, 2023
Published: September 2, 2023

https://doi.org/10.1021/acs.jpcc.3c03521
J. Phys. Chem. C 2023, 127, 18036−18042

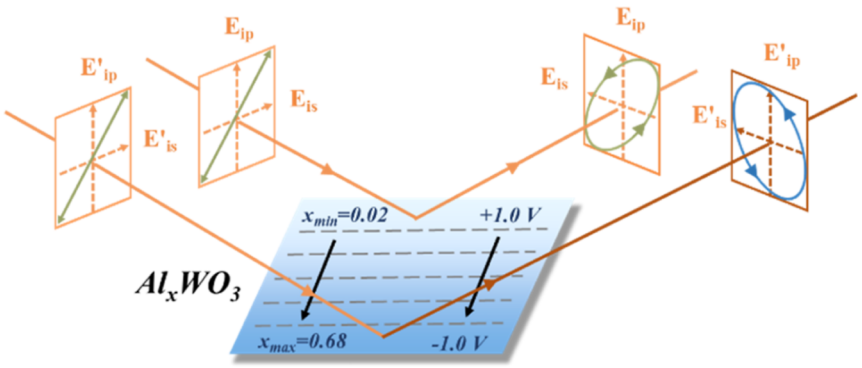

Figure 1. Schematic diagram of tunable optical constants of Al_xWO_3 in the WO_3 thin films under various applied voltages via SE.

higher charge capacity than the monovalent ion (Li^+).[17] Illumining ion-induced optical constants' change of the interface between the WO_3 electrode and the electrolyte is an essential means of improving the EC performance of the WO_3 thin films. Using spectroscopic ellipsometer (SE) based on amplitude ratio and phase difference of reflected polarized light is currently the most widely used approach for its faster, more accurate, and non-destructive merits, which is one of the most suitable methods for investigating materials' surface and interface properties.[18−21] When Al^{3+}-based electrolytes are used to form aluminum tungsten bronzes (Al_xWO_3), the resulting interfacial layer provides a reversible internal interface to WO_3 that external potentials can modulate. Analysis of optical constants of WO_3 thin films in the system of an Al^{3+}-based electrolyte is very significant owing to it being crucial in developing EC devices.

Herein, we demonstrate an optical test designed for tunable optical constants of aluminum tungsten bronzes using an electron beam evaporated nanocrystal-in-glass WO_3 thin film as a typical EC electrode and 0.1 M $Al(ClO_4)_3$-PC as the Al^{3+}-based electrolyte, as shown in Figure 1. X-ray photoelectron spectroscopy has been carried out to confirm a reversible transformation of components of the interface at various colored and bleached states. Our findings fill the gap of optical constants in an Al_xWO_3 EC system and we believe that the significant capacity of Al^{3+} to modulate optical constants at low external voltages allows for energy savings and longer cycle life compared to other ions, as long as the requirements for optical constant changes are met.

2. METHODS

2.1. Synthesis. The WO_3 thin films were deposited on the ITO-coated substrates with the substrate heating at 200 °C by an electron beam evaporation technique (MUE-ECO made in ULVAC, Japan). The background pressure was reduced to less than 4.2×10^{-3} Pa, and pressure was maintained at $\sim 4.0 \times 10^{-3}$ Pa during the deposition process. An appropriate amount of pure WO_3 particles with an average diameter of 3 mm in the tungsten crucible were bombarded by an electron beam of 10 kV without any reactive gas. The deposition rate and thickness were controlled at 0.1 nm/s and approximately 600 nm, respectively. 0.1 M aluminum perchlorate nonahydrate [$Al(ClO_4)_3 \cdot 9H_2O$, 99%] dissolved into propylene carbonate (PC), purchased from J&K Scientific and Sinopharm Chemical Reagent Co. Ltd., respectively, was used as the Al^{3+} electrolyte.

2.2. Measurements. The structure of the WO_3 films was analyzed by X-ray diffraction (XRD, Bruker D8 Advance with Cu Kα radiation (λ = 0.154178 nm) and a $\theta-2\theta$ configuration) and high-resolution transmission electron microscopy (HRTEM, JEOL2100). The distribution of valence states and chemical compositions were performed by X-ray photoelectron spectroscopy (XPS) (AXIS UTLTRA DLD), using Al Kα (1486.6 eV) radiation as an X-ray source with a voltage of 15 kV and a power of 120 W at a pressure of $\sim 5 \times 10^{-9}$ Torr. Optical transmittance spectra and optical constants of the thin films under various voltages were measured via UV−vis−IR spectroscopy (PerkinElmer Lambda 950) and with a variable angle SE (M-2000 DI, J. A. Woollam). The colored and bleached process of the films was achieved by an electrochemical workstation (CHI660D, Chenhua, Shanghai) with a traditional three-electrode cell. A platinum sheet and Ag/AgCl were used as the counter electrode and reference electrode, respectively. The chronoamperometry and cyclic voltammetry measurements were carried out by applying a corresponding voltage.

3. RESULTS AND DISCUSSION

The WO_3 thin films deposited on ITO-coated substrates were analyzed using XRD, TEM, and HRTEM measurements to determine their microstructures and morphologies (Figure S1). The XRD pattern of the WO_3 thin film only showed reflections corresponding to the crystalline ITO substrate (Figure S1a), indicating that the thin film is amorphous. Figure S1b,c depicts the TEM and HRTEM images of the WO_3 thin film deposited on the Cu grid, respectively. The WO_3 thin film exhibits dense white spots with an average size of less than 5 nm, illustrating the existence of nanoscale holes. The selected area electron diffraction displayed in Figure S1b as the inset presents diffused halo rings, confirming the amorphous structure characteristic. The HRTEM image (Figure S1c) manifests an obvious fringe pattern with a fringe spacing of 0.387 nm, corresponding to the lattice spacing of the (002) lattice plane of monoclinic WO_3 (PDF# 43-1035). The packing density (P) of the WO_3 film was calculated by the following equation

$$P = \left(\frac{n_f^2 - 1}{n_f^2 + 2}\right)\left(\frac{n_b^2 + 2}{n_b^2 - 1}\right) \quad (1)$$

where n_f and n_b refer to the refractive indices of the sample and the bulk WO_3 ($n_{550\ nm}$ = 2.5),[22] respectively. The refractive indices can be measured by an SE. The P value of the as-deposited WO_3 thin film is calculated to be 81.6%, further indicating that the WO_3 thin film possesses a porous structure. Compared with the crystalline structure, the nanocrystal-in-glass (nanocrystal-embedded amorphous matrix) structure (or called dual-phase structure) effectively increases the reaction

https://doi.org/10.1021/acs.jpcc.3c03521
J. Phys. Chem. C 2023, 127, 18036−18042

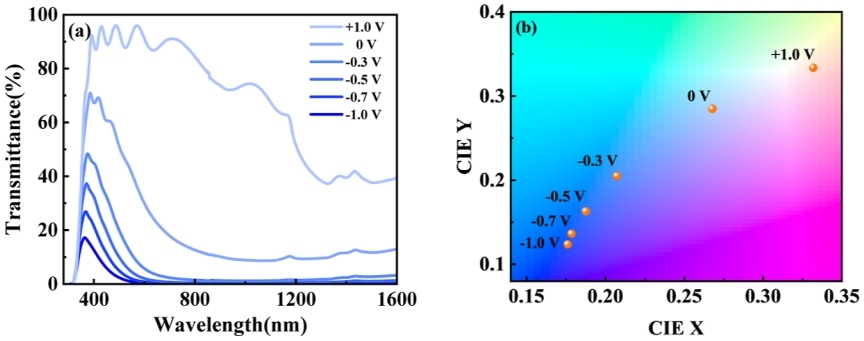

Figure 2. (a) UV−vis−IR transmittance spectra and (b) CIE chromaticity diagram of the colored and bleached WO_3 thin films.

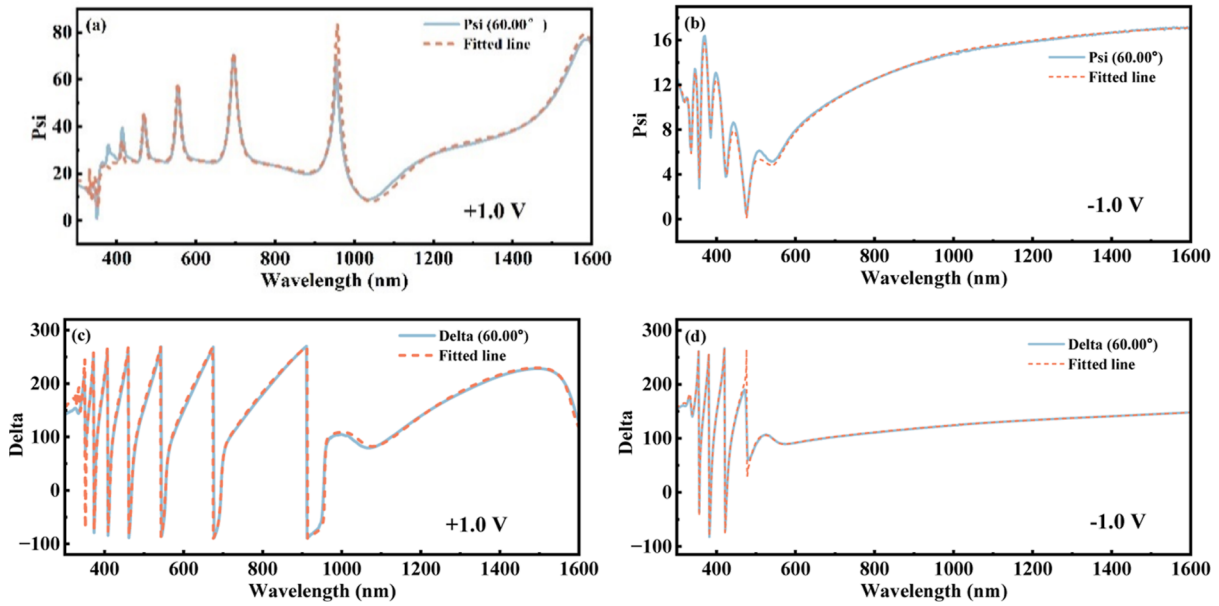

Figure 3. Measured and fitted ellipsometric parameters of the WO_3 thin films in (a,c) the bleached state and (b,d) the fully colored state at 60°.

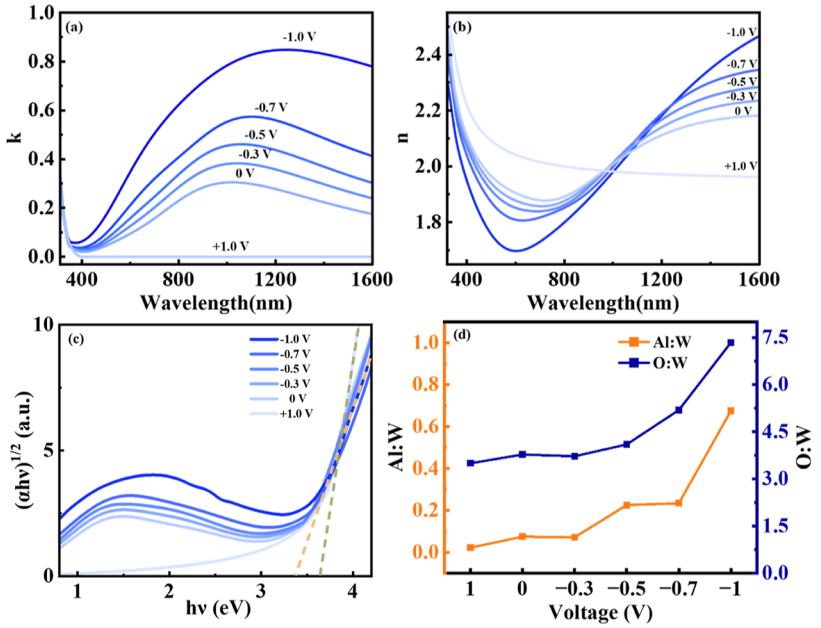

Figure 4. Evolution of extinction coefficient (a) and refractive index (b) of the WO_3 thin films under various applied voltages. (c) Plots of $(\alpha h\nu)^{1/2}$ versus photon energy $h\nu$ of the WO_3 thin films under various colored and bleached states. (d) Applied voltage dependence of the atomic concentration ratio of Al/W and O/W was analyzed by XPS with the aid of respective sensitivity factors.

https://doi.org/10.1021/acs.jpcc.3c03521
J. Phys. Chem. C 2023, 127, 18036−18042

sites of the aluminum ion with W and promotes the diffusion rate of Al^{3+} ions on the interface between the electrolyte and EC thin film.[12,23]

Figure 2a depicts the transmittance spectra of the WO_3 thin films in the bleached state (+1.0 V), fully colored state (−1.0 V), and intermediate states after subtracting the background signal of the electrolyte [0.1 M PC-Al $(ClO_4)_3$ solution]. A considerable transmittance modulation (ΔT) up to 86.5% at 633 nm is obtained between the bleached and fully colored states. While applying the incremental colored voltage, which is equivalent to higher levels of aluminum ion doping in essence, there is a noticeable drop of the transmittance in the visible spectrum, and the surface color of the film transforms from transparent to dark blue, as shown in Figure 2b.

SE measurement was applied to investigate further the optical constants' variation from the WO_3 to Al_xWO_3 caused by the intercalation of Al^{3+} ions. The potentials of different coloration states are set at +1.0, 0, −0.3, −0.5, −0.7, and −1.0 V (versus Ag/AgCl reference electrode). The coloration and bleaching of the films are realized via the chronoamperometry method, and the voltage duration is 40 s. Due to the excellent optical memory effect of the WO_3 thin film[24] and the fast-testing speed of the ellipsometer, there is no significant error in data accuracy due to the bleaching that occurs during the transferring period from the solution to the completion of the test. The ellipsometric data Ψ(Psi) and Δ(delta) have been measured under different voltages of +1.0, 0, −0.3, −0.5, −0.7, and −1.0 V at two different fixed angles of 60 and 70°, respectively. Ψ and Δ have also been simulated with Tauc-Lorentz and Gaussian oscillator dispersion models. The measured and fitted ellipsometric results of the bleached state (+1.0 V) and the fully colored state (−1.0 V) at 60° are displayed in Figure 3, and the remarkable curve coincidence indicates the credibility and accuracy of the fitted data. A similar conclusion has been sorted at the other incident angle of 70° (Figure S2).

Based on Figure 4a, the k value of the film in the bleached state (+1.0 V) equals zero in the wavelength range from 400 to 1600 nm, the same as that of the as-deposited film due to the minimal ions' intercalation (Figure S3). When the as-deposited film is applied to 0 V, the k value significantly rises in both visible and near-infrared regions. According to Figure 4b, the n value displays a downward trend first, leading to the Kramers−Kronig consistency in the visible light wavelength and rises again after reaching the minimum.[18] In addition, the n value will exceed that of the as-deposited state after about 960 nm. As negative applied voltage varies, both n and k possess a greater modulation under a higher colored voltage. Citing instances of refractive index at 0 and −1.0 V, the n of WO_3 changes from 2.03 to 1.89 and 1.70 at 633 nm, 1.96 to 2.18, and 2.47 at 1600 nm. The increase in the extinction coefficient (k) value can be explained by the material's change in energy levels, such as the introduction of defect levels caused by aluminum ion insertion into the thin film and the transition of tungsten's oxidation state from hexavalent to pentavalent.[25] The valence transition can be verified in the XPS analysis in the final section. It should be noted that the results obtained from the ellipsometry reflect the mean values of multiple layers. In reality, there is a gradient distribution of the Al element content in the Al_xWO_3/WO_3 thin film through TOF-SIMS and XPS analyses, as confirmed by Li et al.[26] and our previous work,[23] respectively. Unfortunately, accurate fitting of these results using the gradient layer model poses challenges, primarily attributable to the abrupt transitions observed in the optical constants at the interface. Moreover, it is worth noting that the Δn and Δk at 633 nm of the Al_xWO_3 layers in our work are larger than those of H_xWO_3 and Li_xWO_3 layers,[27−29] indicating that the aluminum tungsten bronzes possess a greater modulation in the optical constants. The larger modulation range of the Al_xWO_3 means that it can achieve the desired modulation capacity at a lower voltage, thereby fulfilling the role of energy conservation. One possible explanation of the better modulation ability is that the small radius (0.053 nm) and stronger electrostatic force make multivalent Al^{3+} react more fully with W reaction sites on tungsten oxide thin films. The tunable optical constants and low thickness expansion may give Al_xWO_3 more advantages in designing precision composite optical films. The tunable optical constants, transmittance, and optical band gap are all caused by the continuously reversible formation of aluminum tungsten bronzes. The optical band gap of the WO_3 thin films is measured and analyzed by an SE. The optical band gap can be calculated according to the following equations[30,31]

$$\alpha(\lambda) = 4k\pi/\lambda \tag{2}$$

$$\alpha h\nu = A(h\nu - E_g)^n \tag{3}$$

where α is the absorption coefficient, h is the Planck constant, ν is the light frequency, A is a proportionality constant, E_g is the optical band gap, λ is the wavelength, and n is a number depending on the nature of transition, which is 1/2 and 2 for the direct band gap semiconductor and indirect band gap semiconductor, respectively. In this work, WO_3 is treated as an indirect band gap semiconductor; hence, n is considered as 2. Various curves of $(\alpha h\nu)^{1/2}$ versus the photon energy $h\nu$ under a corresponding voltage have been calculated as shown in Figure 4c. The optical band gap (E_g) can be obtained through a linear fitting at the beginning of the optical transition of the WO_3 film near the band edge, and the value is equal to the abscissa of the intersection point between the fitting line and the coordinate axis. The optical band gap undergoes a slight decrease from 3.64 eV at the bleached state to 3.38 eV at the fully colored state, and this change is relatively small, similar to the results measured by a UV−vis spectrometer (Figure S4). The phenomenon of decrease in optical band gap may result from the following reasons. On the one hand, there is a transformation in chemical composition of the thin film and introduction of defect levels caused by the incorporation of Al^{3+}, which influences the electronic structure and band gap. On the other hand, the insertion of aluminum ions causes lattice distortion in the original material, altering the atomic spacing and subsequently affecting the change in optical band gap. Besides, a transition in electrical conductivity of conductor aluminum tungsten bronze (Al_xWO_3) from semiconductor tungsten oxide (WO_3) is a simple support for this phenomenon.[32] Combined with the small polaron theory, the essence of the WO_3 EC thin film is the small-polaron hopping and transformation of the tungsten valence state caused by electrons' transfer from oxygen vacancies or ions.[33,34] When the WO_3 thin films are set under a voltage lower than or equal to 0 V (Ag/AgCl as a reference electrode), driven by the applied electric field, the Al^{3+} ions and electrons transfer into the WO_3 films through the electrolyte and external circuit, respectively, according with the classical model of double injection for electrochromism.[35] Also, the variations of optical constants are attributed to the progressive generation

https://doi.org/10.1021/acs.jpcc.3c03521
J. Phys. Chem. C 2023, 127, 18036−18042

Table 1. Specific Thickness Results from SE of the WO_3 Thin Films at Various Voltages

	WO_3					
voltage (V)	+1.0	0	−0.3	−0.5	−0.7	−1.0
thickness (nm)	604.08	608.77	612.14	614.17	615.17	616.91

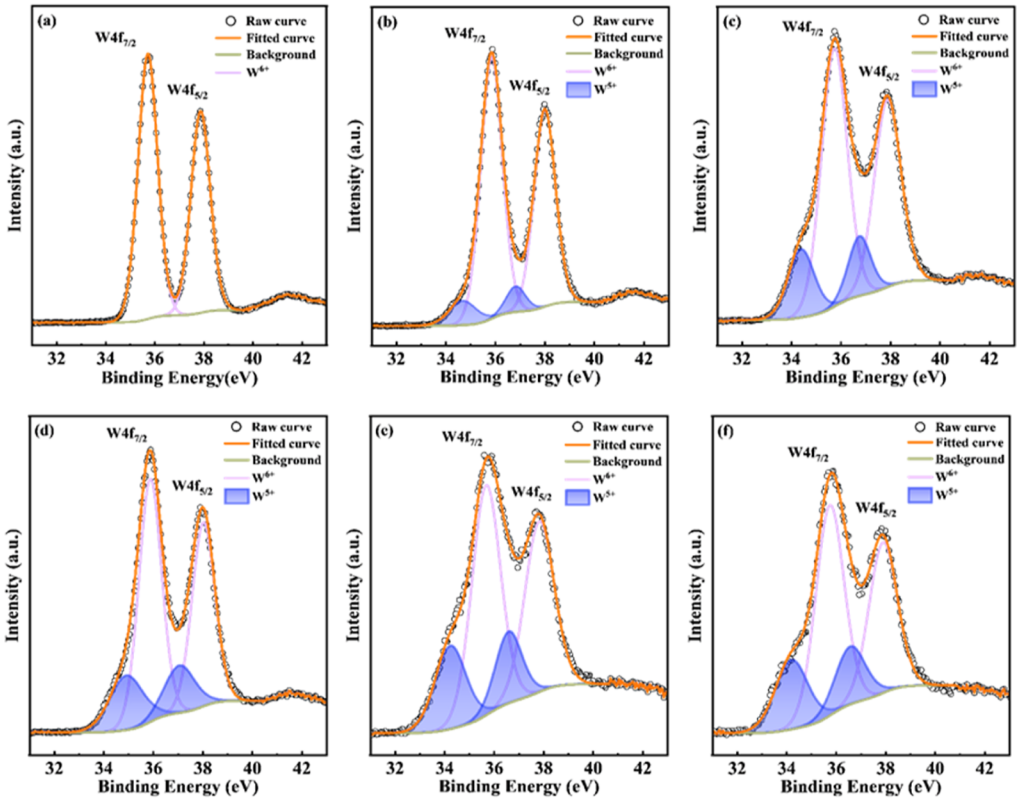

Figure 5. XPS spectra analysis of W_{4f} from the WO_3 thin films at various colored and bleached states of (a) +1.0, (b) 0, (c) −0.3, (d) −0.5, (e) −0.7, and (f) −1.0 V.

of aluminum tungsten bronzes according to the following equation

$$WO_3 + xAl^{3+} + xe^- \leftrightarrow Al_xWO_3 \quad (4)$$

As thin-film components vary, W's valence state constantly changes between pentavalent and hexavalent, essentially resulting in changes in the optical properties of the WO_3 films. For further investigating the chemical state evolution and element content alteration of Al_xWO_3 thin films, XPS analysis was carried out for the WO_3 thin films at various coloration states. Figure 4d compares the content ratio of each element and tungsten element under various applied voltages. With the increment of the negative voltage, the content of aluminum in the Al_xWO_3 layer increases gradually from x = 0.02 at the bleached state (closed to x = 0 at the as-deposited state) to x = 0.68 at the full colored state, confirming the intercalation behavior of Al^{3+} ions. Meanwhile, the ratio O/W also exhibits an upward trend from 3.50 to 7.33 (3.12 at the as-deposited state) due to the adhesion of water vapor while the surface of the thin film was exposed to air.

Table 1 presents the corresponding thickness of the WO_3 film under various voltages of +1.0, 0, −0.3, −0.5, −0.7, and −1.0 V. The increased voltage leads to an increase in the film thickness. With the Al^{3+} ion intercalation, the film gets thicker from 604.08 nm (bleached state) to 616.91 nm (fully colored state), and Δd_{max} = 12.83 nm.

The aluminum ions diffuse into the internal structural framework of the WO_3 film through the free channel distributed disorderly in the amorphous matrix, resulting in the structural volume expansion. The maximum expansion rate originated from Al_xWO_3 is calculated to be approximately 2.12%, less than 3.77% of that from Na_xWO_3 for the WO_3 thin films.[36] During ion insertion, the thin films experience expansion, which generally leads to structural collapse and degradation of the host material, thereby limiting the cycle life of EC films or devices. Nevertheless, maybe due to the smaller ion radius and stronger electrostatic forces,[17] Al^{3+} exerts an effect on stabilizing the host framework, resulting in a lower maximum expansion rate. This provides a reliable explanation for why aluminum-based devices have a longer cycling lifetime. Also, the lower maximum expansion also gives Al_xWO_3 more advantages in precision composite optical film designs.

It is seen from Figure 5 that the spectrum of W_{4f} consists of a single doublet at binding energies of 35.7 and 37.8 eV for electron orbits of $W_{4f7/2}$ and $W_{4f5/2}$, respectively. The area ratio of the peaks of each doublet is $W_{4f7/2}/W_{4f5/2}$ = 4:3 and the orbit separation is 2.15 eV, which is characteristic of WO_3.[37] After deducting the Shirley background, the ratio of W^{6+}/W^{5+} can be calculated from their individual peak areas after taking the corresponding relative sensitivity factor into consideration. When applying +1.0 V to the film, minimal aluminum tungsten bronze is generated due to the participation of minuscule

https://doi.org/10.1021/acs.jpcc.3c03521
J. Phys. Chem. C 2023, 127, 18036−18042

Table 2. Experimental Results from XPS Spectra of W_{4f} from the As-Deposited WO_3 Films and the WO_3 Films in Various Colored and Bleached States of +1.0, 0, −0.3, −0.5, −0.7, and −1.0 V

bond	contents						
		colored and bleached states of potentials (V)					
peak W_{4f}	as-deposited	+1.0 (%)	0 (%)	−0.3 (%)	−0.5 (%)	−0.7 (%)	−1.0 (%)
W_{4f}^{6+}	100	100	89.41	78.71	74.84	71.92	71.64
W_{4f}^{5+}			10.59	21.29	25.16	28.08	28.36
total W_{4f}	100	100	100	100	100	100	100

irreversible aluminum; hence, it is difficult to simulate the presence of W^{5+} in the film as there is barely any content of W^{5+} present. Therefore, the component of the WO_3 film in the bleached state is virtually identical to that of the as-deposited film where evidence of the W^{5+} component is not found (Figure S5). The component of W^{5+} has been discovered when a voltage of 0 V was applied, and its proportion in the total area of the W_{4f} orbit rises as the negative voltage intensity enhances.

Obtained from Table 2, the atom concentration ratio of W^{6+}/W^{5+} is approximately positive infinity and 2.53 for the bleached state and the fully colored state, respectively. Moreover, it is worth noting that the growth rate of the proportion of W^{5+} slows down; finally, there is only an increase of 0.28% as the applied voltage adjusted from −0.7 to −1.0 V. The slowing growth rate means that there is less amount of generated aluminum tungsten bronzes, which is contradictory to the conclusion inferred from the optical constants. There is a reliable explanation that XPS only detects the surface part (<5 nm) of the thin films, where the reaction sites around W tend to be saturated, leading to only a small amount of tungsten valence transition when the negative voltage is further raised. Under the action of the electric field, aluminum ions can enter the deep layer of the thin film through the channel and combine with more W sites to form aluminum tungsten bronze and the embedding depth is about 40.2 nm, described elsewhere in our previous work;[23] thus, there is no saturation effect observed on the optical constants and transmittance with the enhancement of the negative voltage applied to the thin film.

4. CONCLUSIONS

In summary, we have designed a scheme for measuring the tunable optical constants of Al_xWO_3 layers in diverse colored and bleached states over the spectral range of 330−1600 nm by a variable angle SE. Larger optical constants' modulation has been discovered for the nanocrystal-in-glass WO_3 thin films when operated within a higher potential. Further, the Al_xWO_3 layers also present a larger modulation of optical constants than Li_xWO_3 and H_xWO_3 as well as a smaller maximum expansion rate than Na_xWO_3 because of the smaller ion radius and stronger electrostatic force of Al^{3+}. A decrease in the optical band gap of 0.26 eV can be observed in the fully colored state, which may be attributed to the change of valence state and the introduction of defect energy level during the transformation from semiconductor tungsten oxide to conductor aluminum tungsten bronze. As Al_xWO_3 is generated, the ratio of W^{6+}/W^{5+} declines and reaches a minimum of 2.53 at the potential of −1.0 V. These results are helpful for further investigating the optical characterization of the WO_3 and the structural design of EC devices.

■ ASSOCIATED CONTENT

Supporting Information

The Supporting Information is available free of charge at https://pubs.acs.org/doi/10.1021/acs.jpcc.3c03521.

As-deposited WO_3 thin film; ellipsometric parameters at 70°; optical constants of the as-deposited WO_3 thin film; optical band gap using different materials as the baseline; and XPS spectra analysis of the as-deposited WO_3 film (PDF)

■ AUTHOR INFORMATION

Corresponding Author

Hongliang Zhang − *Laboratory of Advanced Nano Materials and Devices, Ningbo Institute of Materials Technology and Engineering, Chinese Academy of Sciences, Ningbo 315201, China*; orcid.org/0000-0002-9295-8683; Phone: +86 574 86688153; Email: zhanghl@nimte.ac.cn

Authors

Kunrun Song − *Faculty of Electrical Engineering and Computer Science, Ningbo University, Ningbo 315211, China; Laboratory of Advanced Nano Materials and Devices, Ningbo Institute of Materials Technology and Engineering, Chinese Academy of Sciences, Ningbo 315201, China*

Shichen Weng − *Faculty of Electrical Engineering and Computer Science, Ningbo University, Ningbo 315211, China; Laboratory of Advanced Nano Materials and Devices, Ningbo Institute of Materials Technology and Engineering, Chinese Academy of Sciences, Ningbo 315201, China*

Jumei Zhou − *Faculty of Electrical Engineering and Computer Science, Ningbo University, Ningbo 315211, China*

Ran Jiang − *Faculty of Electrical Engineering and Computer Science, Ningbo University, Ningbo 315211, China*

Hongtao Cao − *Laboratory of Advanced Nano Materials and Devices, Ningbo Institute of Materials Technology and Engineering, Chinese Academy of Sciences, Ningbo 315201, China*

Complete contact information is available at: https://pubs.acs.org/10.1021/acs.jpcc.3c03521

Notes

The authors declare no competing financial interest.

■ ACKNOWLEDGMENTS

This project is supported by the National Natural Science Foundation of China (61974148), Natural Science Foundation of Zhejiang Province (LY23F040003), and International Cooperation Project of Ningbo City (2023H003).

■ REFERENCES

(1) Mortimer, R. Electrochromic materials. *Chem. Soc. Rev.* **1997**, *26*, 147−156.

(2) Granqvist, C. G.; Azens, A.; Isidorsson, J.; Kharrazi, M.; Kullman, L.; Lindstrom, T.; Niklasson, G. A.; Ribbing, C. G.; Ronnow, D.; Strømme Mattsson, M.; et al. Towards the smart window: progress in electrochromics. *J. Non-Cryst. Solids* **1997**, *218*, 273−279.
(3) Liao, C. C.; Chen, F. R.; Kai, J. J. Electrochromic properties of nanocomposite WO_3 films. *Sol. Energy Mater. Sol. Cells* **2007**, *91*, 1282−1288.
(4) Meenakshi, M.; Gowthami, V.; Perumal, P.; Sivakumar, R.; Sanjeeviraja, C. Influence of dopant concentration on the electrochromic properties of tungsten oxide thin films. *Electrochim. Acta* **2015**, *174*, 302−314.
(5) Cong, S.; Geng, F. X.; Zhao, Z. G. Tungsten Oxide Materials for Optoelectronic Applications. *Adv. Mater.* **2016**, *28*, 10518−10528.
(6) Ganesh, G. P. T.; Deb, B. Designing an All-Solid-State Tungsten Oxide Based Electrochromic Switch with a Superior Cycling Efficiency. *Adv. Mater. Interfaces* **2017**, *4*, 1700124.
(7) Li, Y. T.; Liu, Z. F.; Ruan, M. N.; Guo, Z. G.; Li, X. F. 1D WO_3 Nanorods/2D WO_{3-x} Nanoflakes Homojunction Structure for Enhanced Charge Separation and Transfer towards Efficient Photoelectrochemical Performance. *ChemSusChem* **2019**, *12*, 5282−5290.
(8) Li, Y. T.; Liu, Z. F.; Li, J. W.; Ruan, M. N.; Guo, Z. G. An effective strategy of constructing a multi-junction structure by integrating a heterojunction and a homojunction to promote the charge separation and transfer efficiency of WO_3. *J. Mater. Chem. A* **2020**, *8*, 6256−6267.
(9) Li, T. H.; Zou, Y. J.; Liu, Z. F. Magnetic-thermal external field activate the pyro-magnetic effect of pyroelectric crystal ($NaNbO_3$) to build a promising multi-field coupling-assisted photoelectrochemical water splitting system. *Appl. Catal., B* **2023**, *328*, 122486.
(10) Li, T. H.; Ruan, M. N.; Guo, Z. A.; Wang, C. Y.; Liu, Z. F. Modulation of Lewis and Bronsted Acidic Sites to Enhance the Redox Ability of Nb_2O_5 Photoanodes for Efficient Photoelectrochemical Performance. *ACS Appl. Mater. Interfaces* **2023**, *15*, 11914−11926.
(11) Llordes, A.; Garcia, G.; Gazquez, J.; Milliron, D. J. Tunable near-infrared and visible-light transmittance in nanocrystal-in-glass composites. *Nature* **2013**, *500*, 323−326.
(12) Kim, H.; Choi, D.; Kim, K.; Chu, W.; Chun, D.-M.; Lee, C. S. Effect of particle size and amorphous phase on the electrochromic properties of kinetically deposited WO_3 films. *Sol. Energy Mater. Sol. Cells* **2018**, *177*, 44−50.
(13) Yu, H.; Guo, J. J.; Wang, C.; Zhang, J. Y.; Liu, J.; Zhong, X. L.; Dong, G. B.; Diao, X. G. High performance in electrochromic amorphous WOx film with long-term stability and tunable switching times via Al/Li-ions intercalation/deintercalation. *Electrochim. Acta* **2019**, *318*, 644−650.
(14) Li, H.; Elezzabi, A. Y. Simultaneously enabling dynamic transparency control and electrical energy storage via electrochromism. *Nanoscale Horiz.* **2020**, *5*, 691−695.
(15) Zhang, S. L.; Cao, S.; Zhang, T. R.; Fisher, A.; Lee, J. Y. Al^{3+} intercalation/de-intercalation-enabled dual-band electrochromic smart windows with a high optical modulation, quick response and long cycle life. *Energy Environ. Sci.* **2018**, *11*, 2884−2892.
(16) Guo, J. J.; Wang, M.; Diao, X. G.; Zhang, Z. B.; Dong, G. B.; Yu, H.; Liu, F. M.; Wang, H.; Liu, J. Prominent Electrochromism Achieved Using Aluminum Ion Insertion/Extraction in Amorphous WO_3 Films. *J. Phys. Chem. C* **2018**, *122*, 19037−19043.
(17) Zhang, H. L.; Liu, S.; Xu, T.; Xie, W. P.; Chen, G. X.; Liang, L. Y.; Gao, J. H.; Cao, H. T. Aluminum-ion-intercalation nickel oxide thin films for high-performance electrochromic energy storage devices. *J. Mater. Chem. C* **2021**, *9*, 17427−17436.
(18) Hilfiker, J. N.; Singh, N.; Tiwald, T.; Convey, D.; Smith, S. M.; Baker, J. H.; Tompkins, H. G. Survey of methods to characterize thin absorbing films with Spectroscopic Ellipsometry. *Thin Solid Films* **2008**, *516*, 7979−7989.
(19) Herzinger, C. M.; Johs, B.; McGahan, W. A.; Woollam, J. A.; Paulson, W. Ellipsometric determination of optical constants for silicon and thermally grown silicon dioxide via a multi-sample, multi-wavelength, multi-angle investigation. *J. Appl. Phys.* **1998**, *83*, 3323−3336.
(20) Tompkins, H. G. Industrial applications of spectroscopic ellipsometry. *Thin Solid Films* **2004**, *455−456*, 772−778.
(21) Guo, C.; Kong, M. D.; Gao, W. D.; Li, B. C. Simultaneous determination of optical constants, thickness, and surface roughness of thin film from spectrophotometric measurements. *Opt. Lett.* **2013**, *38*, 40−42.
(22) Sawada, S.; Danielson, G. C. Optical indices of refraction of WO_3. *Phys. Rev.* **1959**, *113*, 1008−1013.
(23) Qiu, D.; Ji, H.; Zhang, X.; Zhang, H.; Cao, H.; Chen, G.; Tian, T.; Chen, Z.; Guo, X.; Liang, L.; et al. Electrochromism of Nanocrystal-in-Glass Tungsten Oxide Thin Films under Various Conduction Cations. *Inorg. Chem.* **2019**, *58*, 2089−2098.
(24) Yao, Y. J.; Zhao, Q.; Wei, W.; Chen, Z.; Zhu, Y.; Zhang, P.; Zhang, Z. T.; Gao, Y. F. WO_3 quantum-dots electrochromism. *Nano Energy* **2020**, *68*, 104350.
(25) Arslan, M.; Firat, Y. E.; Tokgoz, S. R.; Peksoz, A. Fast electrochromic response and high coloration efficiency of Al-doped WO_3 thin films for smart window applications. *Ceram. Int.* **2021**, *47*, 32570−32578.
(26) Li, H.; Firby, C. J.; Elezzabi, A. Y. Rechargeable Aqueous Hybrid Zn^{2+}/Al^{3+} Electrochromic Batteries. *Joule* **2019**, *3*, 2268−2278.
(27) Yuan, G.; Hua, C.; Huang, L.; Defranoux, C.; Basa, P.; Liu, Y.; Song, C.; Han, G. Optical characterization of the coloration process in electrochromic amorphous and crystalline WO_3 films by spectroscopic ellipsometry. *Appl. Surf. Sci.* **2017**, *421*, 630−635.
(28) Lagier, M.; Bertinotti, A.; Bouvard, O.; Burnier, L.; Schüler, A. Optical properties of in vacuo lithiated nanoporous WO_3:Mo thin films as determined by spectroscopic ellipsometry. *Opt. Mater.* **2021**, *117*, 111091.
(29) von Rottkay, K.; Rubin, M.; Wen, S. J. Optical indices of electrochromic tungsten oxide. *Thin Solid Films* **1997**, *306*, 10−16.
(30) Schirmer, O. F.; Wittwer, V.; Baur, G.; Brandt, G. Dependence of WO_3 Electrochromic Absorption on Crystallinity. *J. Electrochem. Soc.* **1977**, *124*, 749−753.
(31) Zou, Y. S.; Zhang, Y. C.; Lou, D.; Wang, H. P.; Gu, L.; Dong, Y. H.; Dou, K.; Song, X. F.; Zeng, H. B. Structural and optical properties of WO_3 films deposited by pulsed laser deposition. *J. Alloys Compd.* **2014**, *583*, 465−470.
(32) Jiao, Z.; Wang, J.; Ke, L.; Liu, X.; Demir, H. V.; Yang, M. F.; Sun, X. W. Electrochromic properties of nanostructured tungsten trioxide (hydrate) films and their applications in a complementary electrochromic device. *Electrochim. Acta* **2012**, *63*, 153−160.
(33) Triana, C. A.; Granqvist, C. G.; Niklasson, G. A. Electrochromism and small-polaron hopping in oxygen deficient and lithium intercalated amorphous tungsten oxide films. *J. Appl. Phys.* **2015**, *118*, 024901.
(34) Niklasson, G. A.; Berggren, L.; Larsson, A.-L. Electrochromic tungsten oxide: the role of defects. *Sol. Energy Mater. Sol. Cells* **2004**, *84*, 315−328.
(35) Faughnan, B. W.; Crandall, R. S.; Heyman, P. M. Electrochromism in wo_3 amorphous films. *RCA Rev.* **1975**, *36*, 177−197.
(36) Zimmer, A.; Gilliot, M.; Tresse, M.; Broch, L.; Tillous, K. E.; Boulanger, C.; Stein, N.; Horwat, D. Coloration mechanism of electrochromic Na_xWO_3 thin films. *Opt. Lett.* **2019**, *44*, 1104−1107.
(37) Leftheriotis, G.; Papaefthimiou, S.; Yianoulis, P.; Siokou, A. Effect of the tungsten oxidation states in the thermal coloration and bleaching of amorphous WO_3 films. *Thin Solid Films* **2001**, *384*, 298−306.

https://doi.org/10.1021/acs.jpcc.3c03521
J. Phys. Chem. C 2023, 127, 18036−18042